A Dual-Modality Origami Paper Biosensor for Direct Detection of Borrelia OspC

Antigen-based detection in early Lyme borreliosis, prior to seroconversion

Saba Niaz

PhD Researcher · supervised by Dr Ojodomo Achadu
National Horizons Centre, Teesside University

Learning objectives

1. **Understand the diagnostic gap**

   Delayed seroconversion, cross-reactivity, seronegative cases

2. **See how a CQD biosensor is built and validated**

   Material selection, binding confirmation, MIP-based selectivity

3. **Learn why a second, independent signal matters**

   Antigen-specific fingerprinting for multiplexed detection

4. **Know where this is heading**

   Full antigen panel, clinical validation, point-of-care deployment

Serological diagnosis is insensitive in early infection

Standard two-tier serology detects host antibodies, which require 2–6 weeks to reach detectable titres.

4 in 10

early-stage infections still missed

Even IGeneX's FDA-cleared multi-strain immunoblot (2026), the newest advance, raised early detection from 30% to 58%. It is still reading antibodies.

1. **Delayed antibody response**

   Nothing to detect during the window when treatment works best.

2. **Cross-reactivity**

   Other infections trigger false positives; interpretation is subjective.

3. **Seronegative patients**

   Some never mount a detectable antibody response at all.

The gap this platform targets: detect the antigen itself, before the immune system responds.

A single substrate providing two orthogonal detection signals

Sample applied once; folding routes it sequentially to two independent detection zones.

A — **Sample inlet**

sample

B — **Flow / fold**

C — **Fluorescence zone**

CQD–MIP

D — **SERS zone**

Au nanoparticles

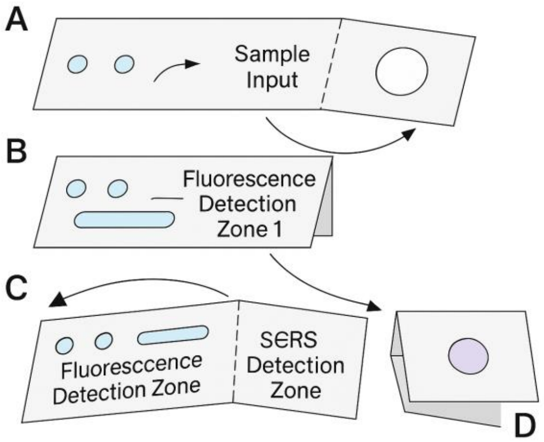

Origami paper–based diagnostic device

SIGNAL 1 · Fluorescence

CQD–MIP capture; quenching reports that OspC has bound.

SIGNAL 2 · SERS

Vibrational fingerprint confirms the identity of the bound antigen.

Unfolded paper strip — folding brings each zone into contact with the sample in sequence

PART ONE

The Fluorescence Arm

Carbon quantum dots as the reporter · molecularly imprinted polymers for selectivity

Carbon quantum dots as fluorescent transducers

Sub-10 nm carbon nanoparticles with tunable surface chemistry and high photostability.

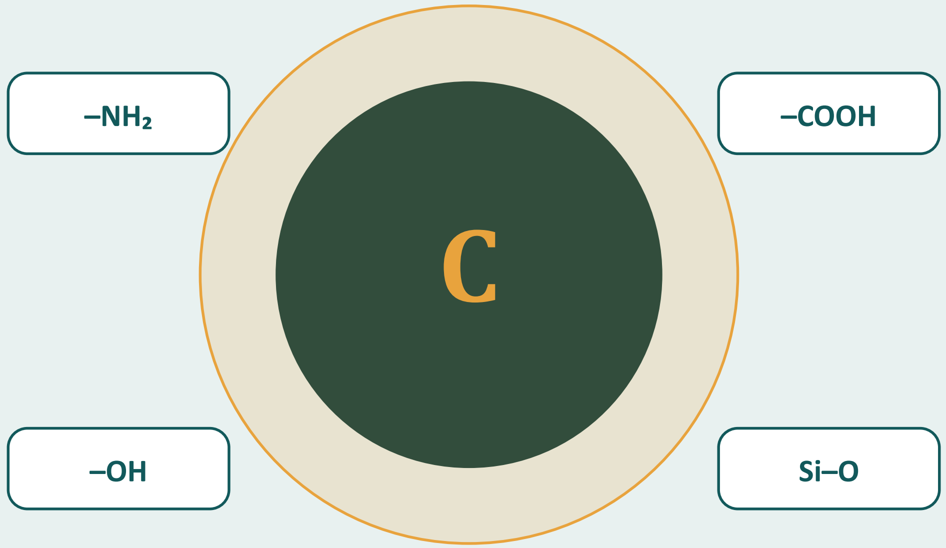

Surface functional groups are where the antigen interacts

Nanoscale

Under 10 nm — small enough to disperse freely and present a large surface area.

Bright and photostable

Strong fluorescence that resists photobleaching, unlike organic dyes.

Low toxicity

Carbon-based — avoids the heavy metals used in conventional semiconductor dots.

Tunable surface

Doping and functionalisation set both the brightness and what the surface will bind.

Why they suit a paper device: bright, cheap, stable at room temperature, and readable by eye under UV.

Synthesis of the Quantum Dots

Urea-CQDs (lead) vs. CuInS/ZnS QDs (semiconductor comparator) - APTES- and EDA-CQDs also screened, see comparison.

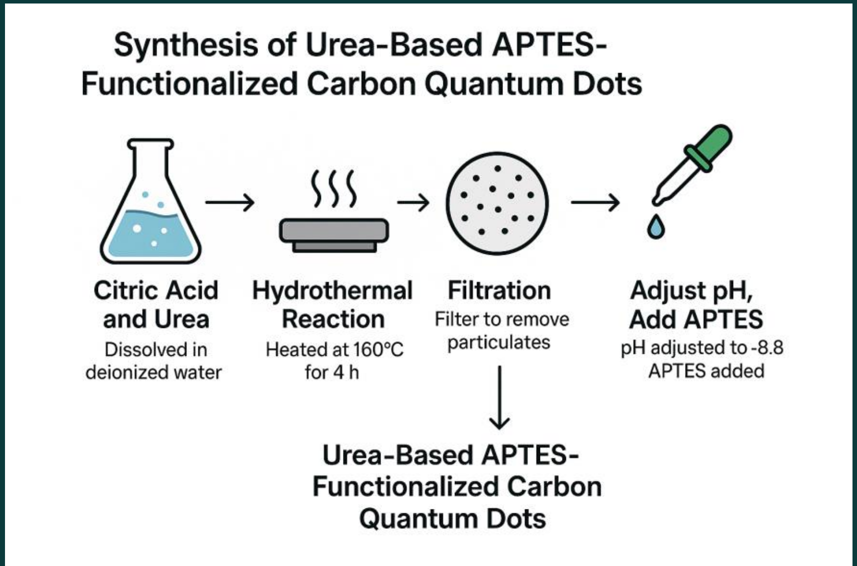

Urea-CQDs

Citric acid + urea, then APTES

Dual N-doping + silane

LEAD

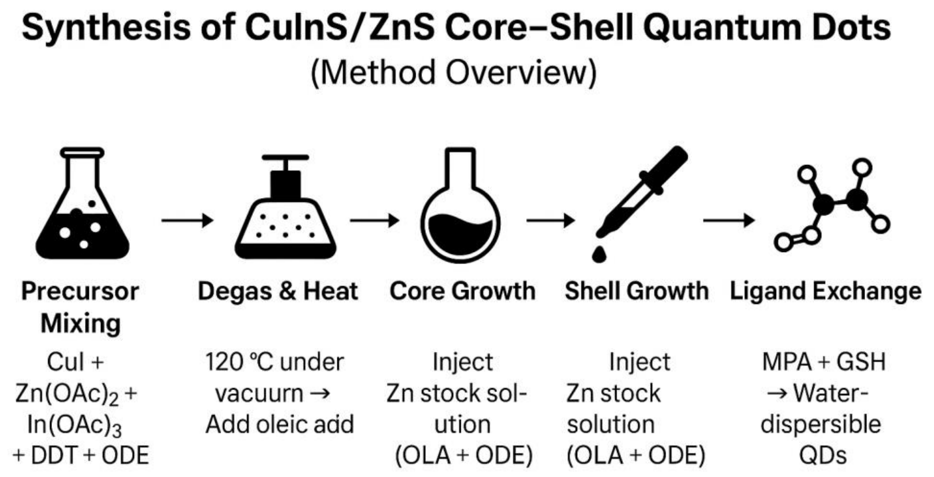

CuInS/ZnS QDs

Organometallic, 230 °C, ligand exchange

Semiconductor comparator

Both routes are bottom-up and low-cost - no specialist fabrication equipment required.

Optical characterisation of the four candidates

UV-Vis absorbance and fluorescence emission recorded for each material.

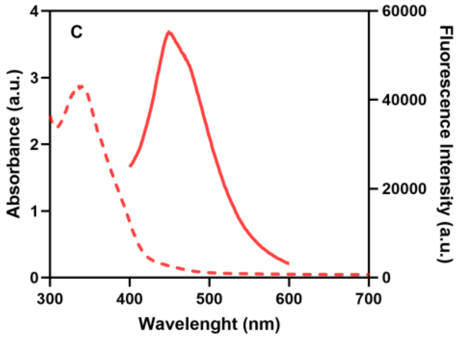

A APTES-CQDs

Abs ~340 nm · Em ~445 nm

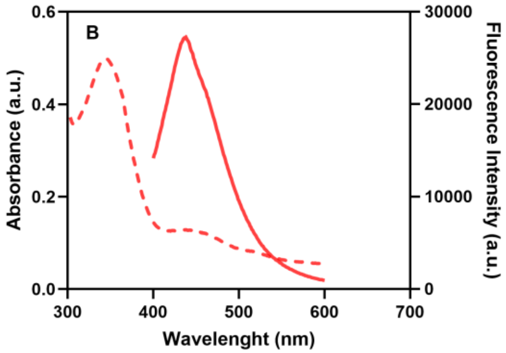

B EDA-CQDs

Abs ~335 nm · Em ~440 nm

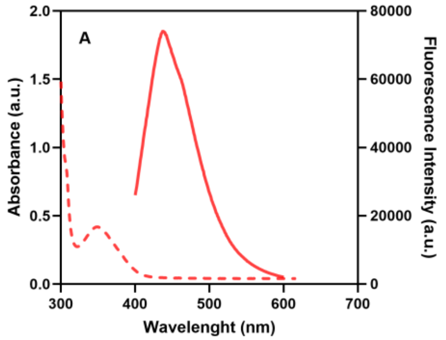

C Urea-CQDs

Abs ~340 nm · Em ~455 nm

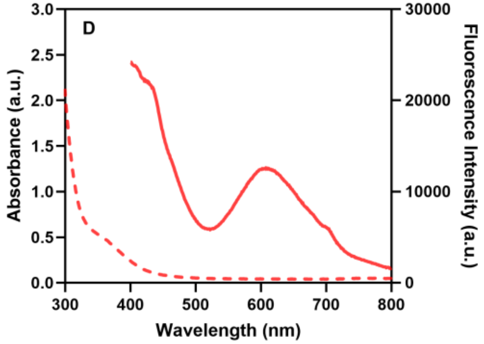

D CuInS/ZnS

Broad abs <400 nm · Em ~610 nm

Urea-CQDs combine the highest quantum yield (59%) with emission well separated from the excitation source.

Physicochemical characterisation of CQD derivatives

Transmission electron microscopy, dynamic light scattering and zeta potential analysis

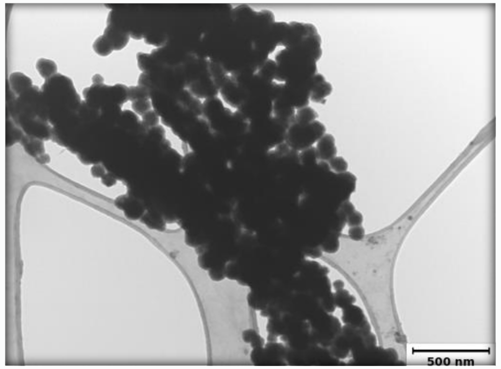

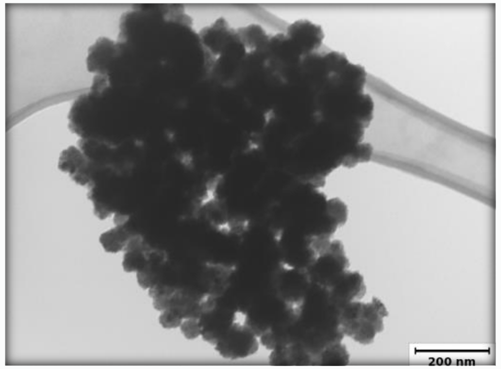

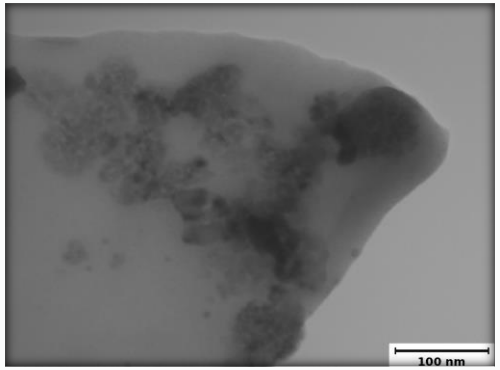

TEM · APTES-, EDA- and Urea-CQDs

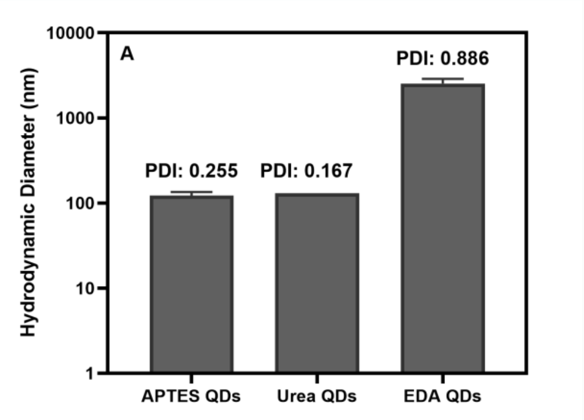

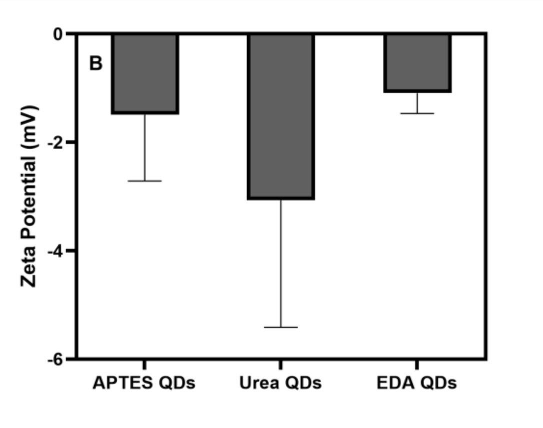

DLS size + PDI · zeta potential

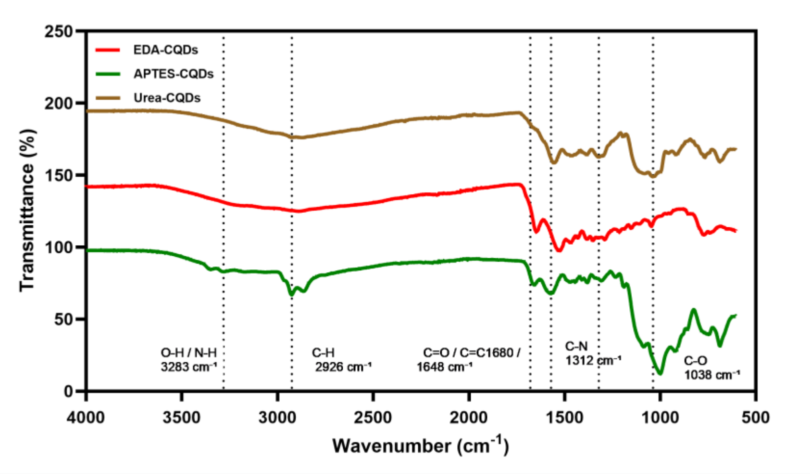

FTIR – Fourier transform infrared spectroscopy

Comparative screening identifies Urea-CQDs as lead material

Selection based on quantum yield, colloidal stability and inter-assay reproducibility.

LEAD
Urea-CQDs
QY 59% · PDI 0.167

Highest quantum yield, best colloidal stability, reproducible quenching.

COMPARATOR
EDA-CQDs
QY 36% · PDI 0.886

Heavy aggregation (2535 nm) limits reproducibility.

ON HOLD
APTES-CQDs
PDI 0.255

No biosensing dataset; deprioritised.

REVISIT
CuInS/ZnS QDs
Distinct ~610 nm emission

Strongest raw quenching in early screen; low synthesis yield.

Quantum yield (%)

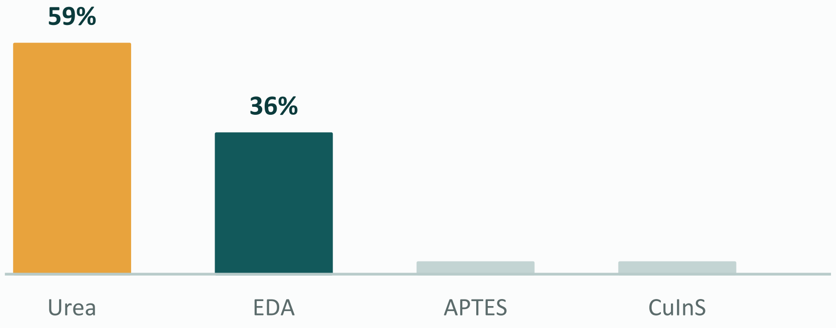

Hydrodynamic diameter (nm)

EDA-CQDs aggregate extensively — roughly 20× larger than the other derivatives

Urea-CQDs carried forward — highest quantum yield with the colloidal stability a paper device requires.

Fluorescence quenching assay design

OspC interaction with the CQD surface produces a concentration-dependent decrease in emission intensity.

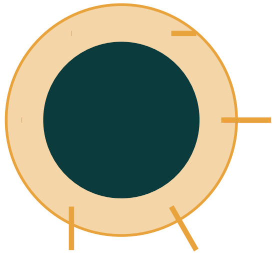

Urea-CQD alone

Strong emission at 445 nm

+ OspC →

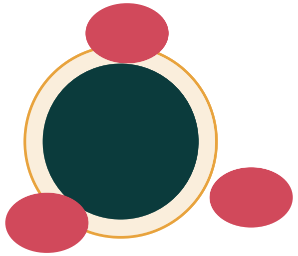

OspC bound

Emission reduced in proportion to [OspC]

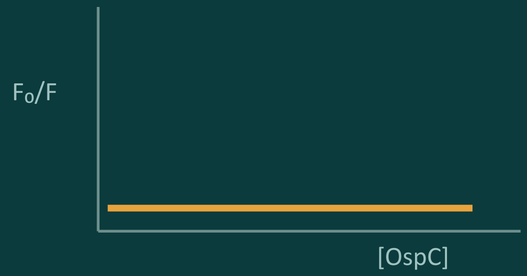

Quantification

Slope of F_0/F vs [OspC] gives K

Assay conditions

80 µL Urea-CQD + 20 µL OspC per well · 30 min incubation · λ_{ex} 350 nm, emission 400–600 nm · triplicate (n = 3) with eight replicate blanks on every plate

Concentration-dependent quenching of Urea-CQDs by OspC

Reproducible across four independent experiments (9.1–69.1 nM OspC, n = 3 per point).

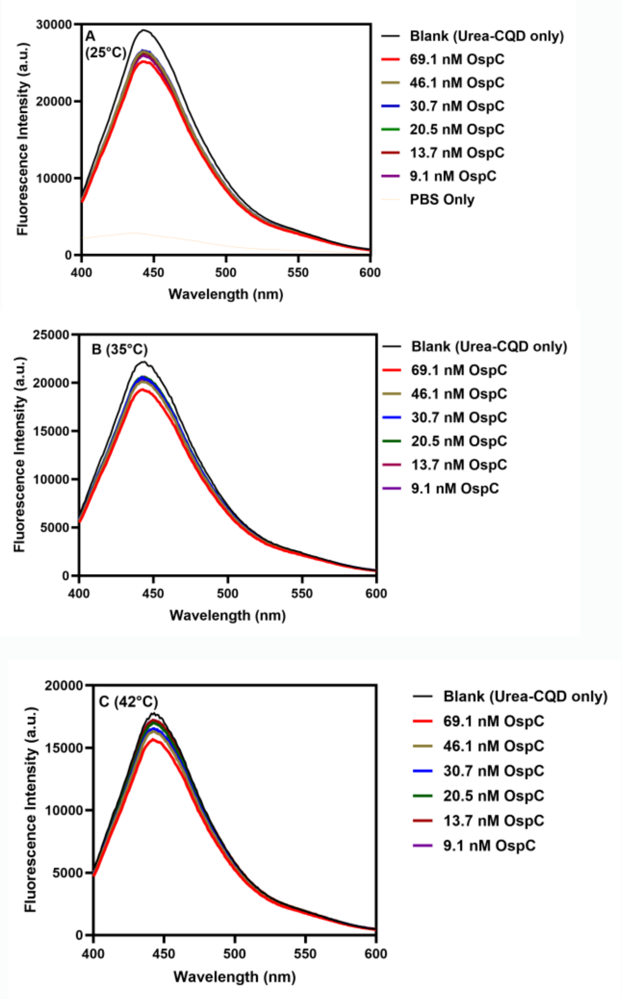

25 °C

35 °C

42 °C

Emission spectra at 25, 35 and 42 °C

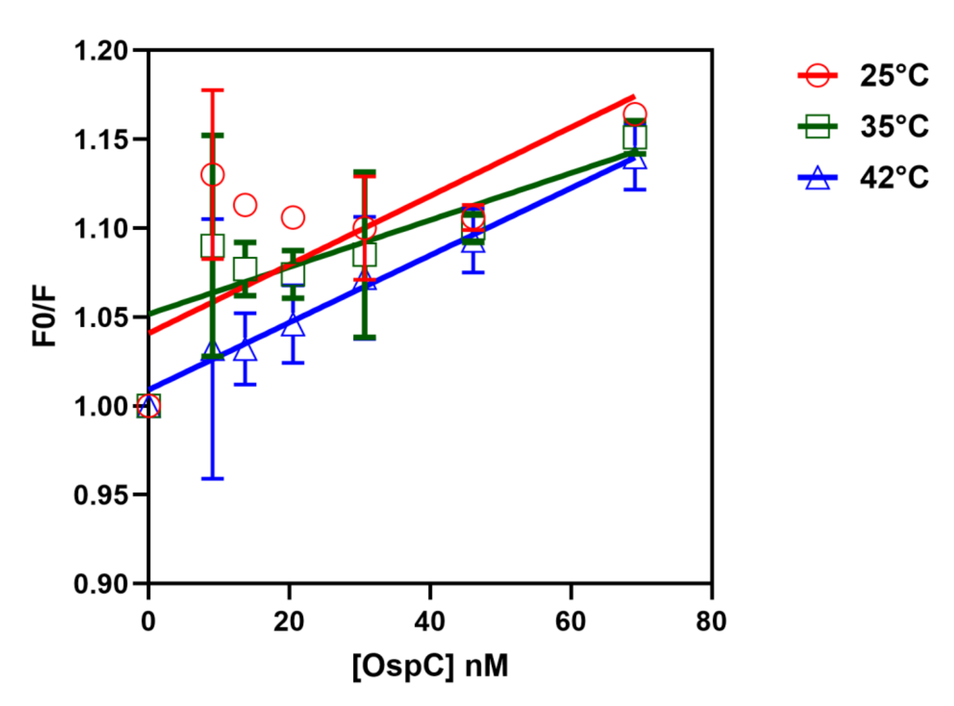

Stern–Volmer, 25 / 35 / 42 °C (mean ± SD, n = 3)

~18%

quenching

at 69.1 nM OspC

0.991

R^2 at 42 °C

vs 0.31 at 25 °C

n = 4

independent runs

16.7 · 17.2 · 19.8 · 18.4%

Temperature dependence indicates a dynamic quenching mechanism

In the absence of time-resolved instrumentation, temperature-dependent Stern–Volmer analysis discriminates static from dynamic quenching.

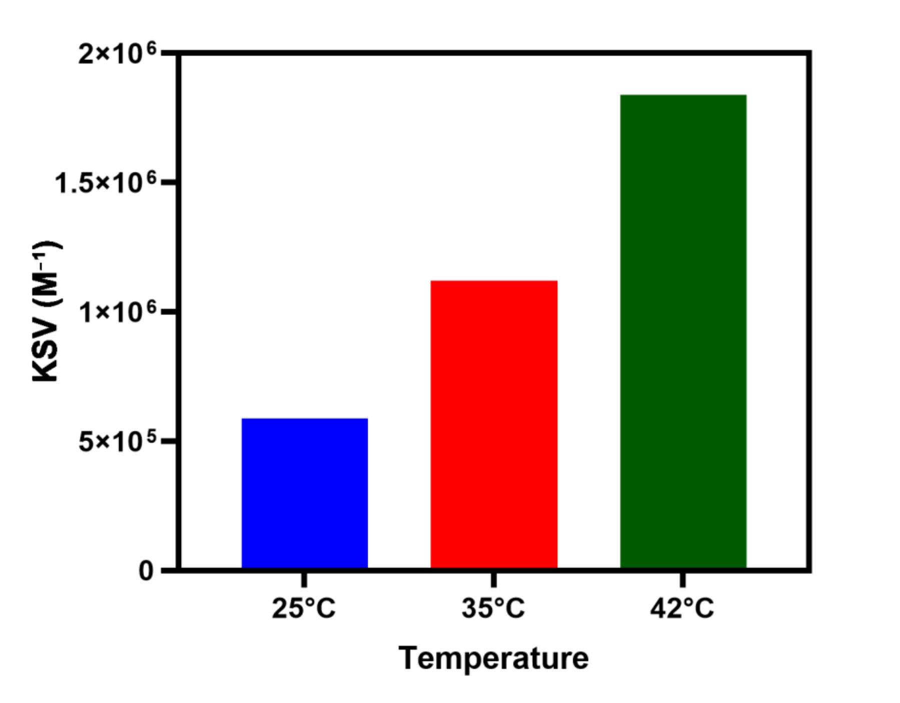

K SV rises 3-fold with temperature

$5.87 \times 10^5 \rightarrow 1.84 \times 10^6\ M^{-1}$ (25 °C → 42 °C)

An increasing Stern–Volmer constant with temperature is the signature of dynamic, collisional quenching — not static ground-state complex formation.

This corrected our earlier assumption.

We had proposed static quenching. The temperature series says otherwise — and data quality improved markedly at 42 °C (R^2 0.31 → 0.99), which also points to a better working temperature for the assay.

Molecular imprinting confers target selectivity

The CQD transduces the signal; the imprinted cavity determines which analyte is recognised.

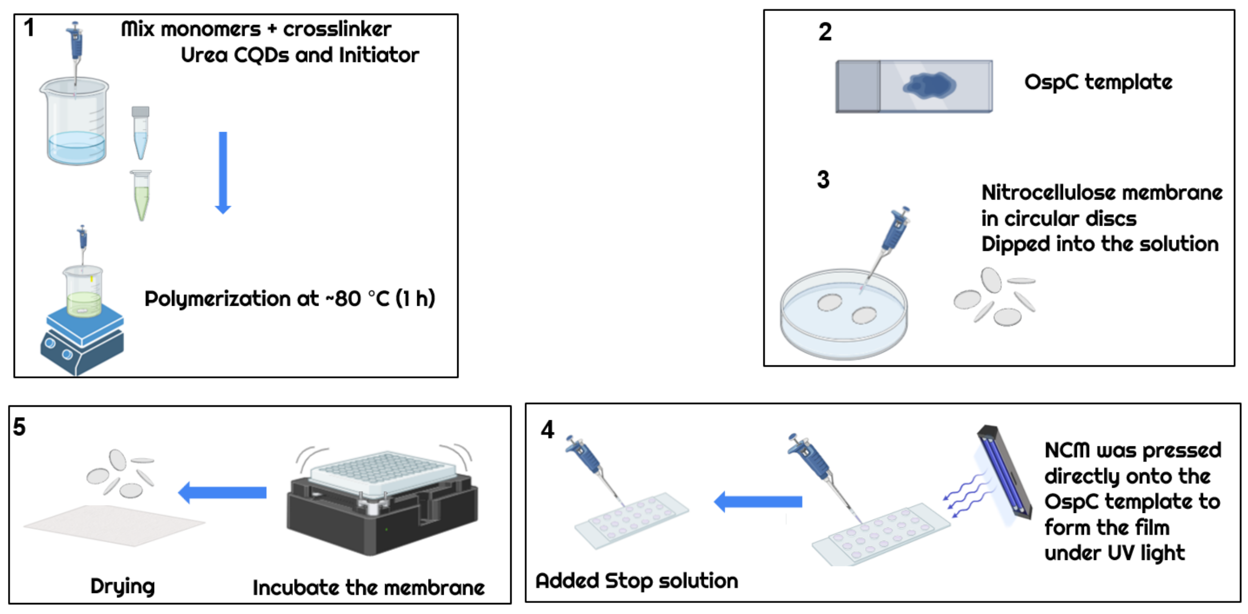

Fabrication: template → polymerisation → template removal → rebinding

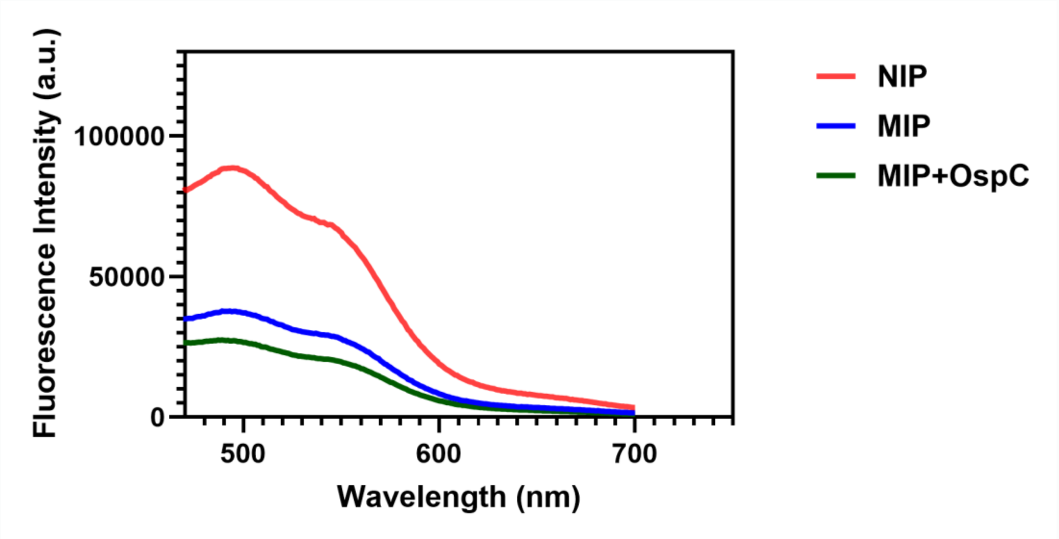

MIP Spectra

NIP baseline

highest signal — no imprinted cavities

Template removed

signal drops as cavities open

OspC rebound

further quenching — selective recapture

FTIR confirms OspC incorporation within the imprinted membrane

Independent spectroscopic confirmation of template retention, complementary to the fluorescence response.

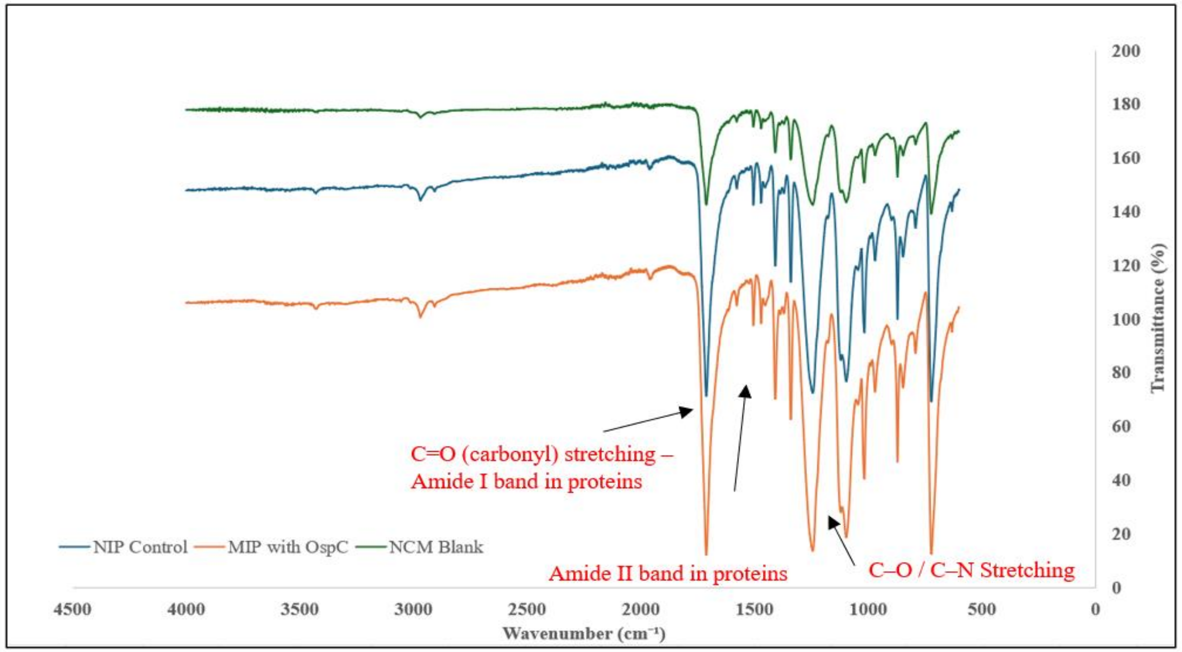

FTIR spectra: NIP control, MIP with OspC, and blank nitrocellulose membrane

Amide I

C=O carbonyl stretching — the protein backbone signature

Amide II

N–H bending, present only where protein is retained

C–O / C–N

Polymer matrix bands, common to MIP and NIP

Amide I and II appear in the OspC-loaded membrane and are absent from the blank — the protein is physically there.

Antibody-mediated fluorescence recovery

Metal-ion quenching followed by anti-OspC antibody addition produces partial signal restoration.

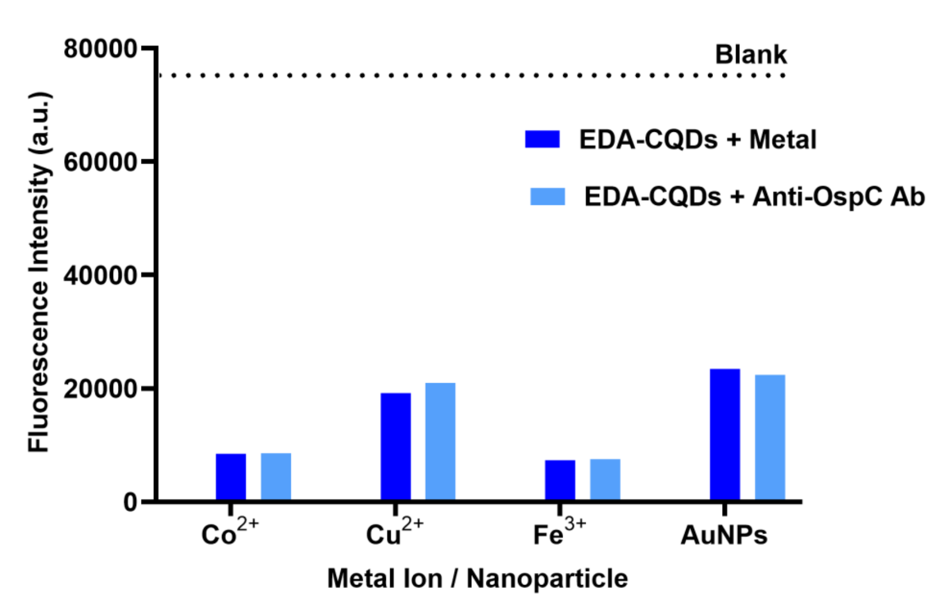

(A) EDA-CQDs

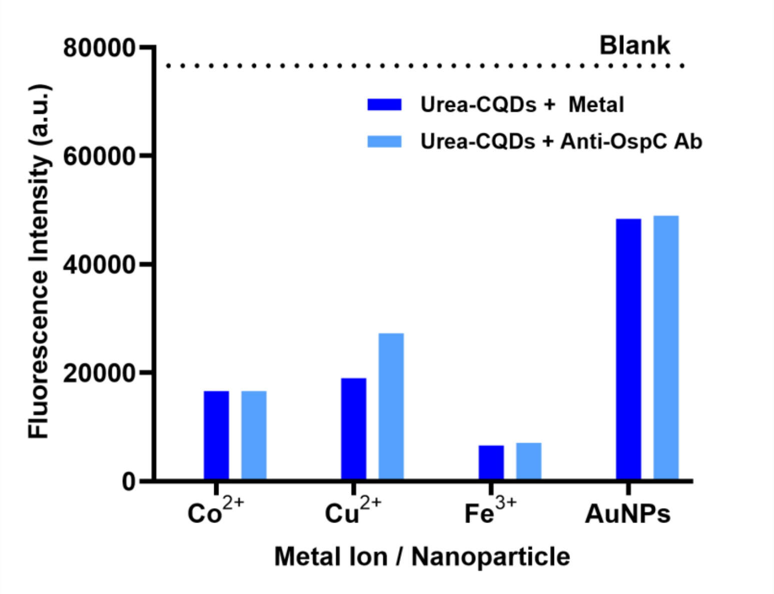

(B) Urea-CQDs

Fe^{3+} quenches most strongly (~92%); anti-OspC antibody at 200 nM drives partial recovery — most pronounced in Cu^{2+}-quenched systems — confirming the antibody-triggered release mechanism.

PART TWO

The SERS Arm

Fluorescence says something bound. Raman says what bound.

Rationale for a second, orthogonal detection modality

Vibrational fingerprinting provides analyte-specific confirmation and enables multiplexed detection.

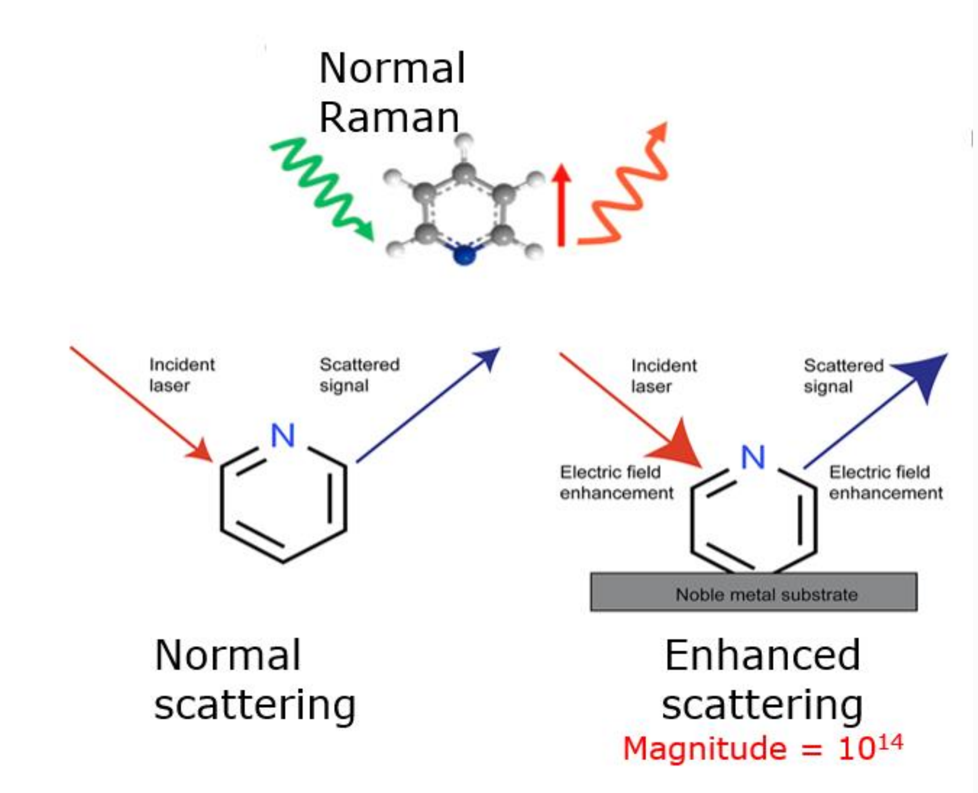

Plasmonic gold amplifies a normally weak Raman signal

Specificity

A Raman fingerprint identifies the molecule, not just its presence.

Amplification

Gold nanoparticles enhance the signal by up to $10^{14}\times$.

Multiplexing

OspC, VlsE and Flagellin read simultaneously on one strip.

Built on proven work

Adapted from our group's validated SERS immunosensor (Nwahara, Niaz et al., Sens. Diagn. 2026).

Extension to the full Borrelia antigen panel

Cross-reactivity assessment and multi-genospecies validation across three European genospecies.

Antigen	Genospecies	Role in validation
OspC	*B. burgdorferi*	**MIP template — validated**
VlsE	*B. burgdorferi*	Late-stage marker; selectivity control
p41 Flagellin	*B. burgdorferi*	Earliest antibody marker; control
OspC	*B. afzelii*	UK-dominant strain; cross-reactivity
Flagellin	*B. garinii*	UK-dominant strain; cross-reactivity

WHY IT MATTERS

3

European genospecies

A test that recognises only B. burgdorferi would miss much of the UK and European disease burden.

Detecting all three European genospecies matters clinically — B. afzelii and B. garinii dominate UK and European cases.

Translational significance

Direct antigen detection alters both the diagnostic window and the patient population that can be tested.

Patients

Earlier diagnosis, before neurological or cardiac complications develop — and without repeat blood draws over weeks.

Clinicians

A test that does not wait for an antibody response. Usable at the point of care, in GP practices and endemic regions.

Scientists

A validated dual-modality template spanning multiple genospecies — transferable to other hard-to-diagnose infections.

Next: complete the triplicate calibration at optimised pH, extend to VlsE and Flagellin, and take the SERS arm from substrate characterisation to antigen-specific fingerprints.

References

1. El-Husseini, D. M., Elmasry, D. M. A., Kassem, S., Hamdy, M., Selim, K. M., & Shahein, M. (2024). Development of a paper-based fluorescent carbon quantum dots MIPs sensor for selective detection of lumpy skin disease virus. *RSC Advances*. https://doi.org/10.1039/D4RA04895D
2. Turkevich, J., Stevenson, P. C., & Hillier, J. (1951). A study of the nucleation and growth processes in the synthesis of colloidal gold. *Discussions of the Faraday Society, 11*, 55-75. https://doi.org/10.1039/DF9511100055
3. Tabb, J. S., Rapoport, E., Han, I., Lombardi, J., & Green, O. (2022). An antigen-targeting assay for Lyme disease: Combining aptamers and SERS to detect the OspA protein. *Nanomedicine: Nanotechnology, Biology, and Medicine, 41*, 102528. https://doi.org/10.1016/j.nano.2022.102528
4. Narasimhan, S., Fikrig, E., et al. (2000). Variations in Barbour-Stoenner-Kelly culture medium modulate infectivity and pathogenicity of *Borrelia burgdorferi* clinical isolates. *Infection and Immunity, 68*(2), 515-519.
5. Fish, D., & Shea, J. J. (2004). Laboratory maintenance of *Borrelia burgdorferi*. *Current Protocols in Microbiology, 12C*.1.1-12C.1.12.
6. Wang, Y., Yan, X., Chen, X., et al. (2019). Development and application of aptamer-based surface-enhanced Raman scattering sensors. *Sensors, 19*(17), 3806.
7. ID-FISH Technology & IGeneX Inc. (2026). Single-step immunoblot improves early-stage Lyme disease detection. *Microbiology Spectrum.*

Thank you

Questions welcome

Saba Niaz

National Horizons Centre · Teesside University
Supervisor: Dr Ojodomo Achadu